

Macro-Micro Inference: Robust Synaptic Classification via Spike-Triggered Extrapolation*

Emilio De Santis

Dipartimento di Matematica, Sapienza Università di Roma
Piazzale Aldo Moro, 5, 00185, Rome, Italy
desantis@mat.uniroma1.it, emilio.desantis@uniroma1.it

March 19, 2026

Abstract

This work introduces a framework for reconstructing the interaction graph of neuronal networks modeled as multivariate point processes. The methodology performs bivariate inference, identifying synaptic links exclusively from the spike trains of a pair of neurons, without requiring observations of the remaining network activity. We propose a Macro-Micro Extrapolation algorithm to address data sparsity at the micro-scale, inferring synaptic interactions in the limit $\Delta \rightarrow 0^+$. A key contribution is the Spike-Triggered Estimator, which leverages the local reset property of Galves-Löcherbach dynamics to decouple local synaptic jumps from higher-order network contributions, significantly reducing estimation variance and eliminating spurious dependencies on baseline firing intensities. By employing an adaptive hybrid logic that switches between sample averaging and our novel Pyramid Extrapolation, we ensure robust classification of excitatory, inhibitory, and null connections even in low signal-to-noise regimes. The framework’s scalability and precision are validated by numerical results on dense cliques and structured layered networks, achieving perfect classification accuracy across diverse topological motifs.

Keywords: Neuronal networks, multivariate point processes, stochastic processes with memory of variable length, interaction graphs, statistical model selection.

1 Introduction

The identification of the underlying interaction graph between neurons, based on the recording of spike train time series, remains a fundamental challenge in neuroscience [1, 3, 4, 5]. Understanding how the activity of one neuron influences another—through excitatory or inhibitory connections—requires statistical models capable of capturing ultra-rapid temporal dynamics, which are often confounded by high variance in low-intensity regimes. In recent years, functional connectivity has been studied primarily through models that integrate diverse observed signals, such as brain rhythms and neuronal spikes [13]. Our approach, however, focuses exclusively on spiking data—the only signal typically available in large-scale extracellular recordings.

*Dedicated to the memory of Antonio Galves (1943–2023), a mentor and collaborator whose brilliance continues to guide this field.

We focus our study on the continuous-time Galves-Löcherbach model (see [7, 10]) to present our techniques for identifying synaptic connections between neurons. Although we believe our methods are sufficiently general and robust, in this paper we apply them to a single model to avoid complexities that would obscure the simulation methods. We highlight, as a key strength, that our statistics identify the presence of a synaptic link between two specific neurons using only their spiking information—an information set that is, in a sense, minimal. Specifically, this work builds upon the research in [1], providing a refined construction of the estimators and extending the analytical framework to include rigorous statistical error bounds for synaptic classification.

A primary difficulty inherent to the methodology in [1] is that the statistical validity of the inference is strictly tied to the choice of an observation window Δ that is sufficiently small to minimize the approximation bias. This requirement, in turn, leads to the extreme sparsity of the associated counting measure, as the statistics defined in [1] are based on the ratio between sums of Bernoulli random variables whose success parameters are $\Theta(\Delta^2)$. Consequently, since asymptotic unbiasedness of the estimator constrains the analysis to such a micro-scale, an exceptionally long observation time would be required to obtain statistically significant results.

To address the statistical challenges of micro-scale analysis, focusing on synaptic connection classification, this paper introduces a structured framework based on two distinct statistics and two different methodological approaches, leading to four possible analytical combinations. The first statistic is a modified version of the estimator established in [1]. The second statistic introduces a window sampling scheme where observation windows are dynamically anchored to the spikes of the target neuron, using the local reset property of the Galves-Löcherbach dynamics. This second statistic is new, while the first can be seen as a rescaling by a factor of Δ^{-1} of the statistic defined in [1]. While this rescaling is less relevant for direct inference at a single fixed Δ , it becomes fundamental when applying the macro-micro extrapolation algorithm [12, 8, 9]. Indeed, the original statistic proposed in [1] vanishes as $\Delta \rightarrow 0^+$, which would lead to an uninformative degenerate limit regardless of the connection type. In contrast, the rescaling ensures that the statistics converge toward well-defined, non-zero limits that are functionally dependent on the synaptic interaction. This effectively “blows up” the microscopic signal, thus allowing for the identification of excitatory, inhibitory, or null connections in the asymptotic regime.

Table 1: Inference Framework: Statistics and Methods

Sampling Scheme / Method	Single-scale	Macro-Micro Extrapolation
Fixed Grid Sampling	Single Small Δ	Extrapolation
Spike-Triggered Sampling	Single Small Δ	Extrapolation

The methods summarized in Table 1 represent different balances between theoretical generality and statistical efficiency. While the fixed grid sampling (top row) maintains a standard approach to point process discretization, in this work we exclusively investigate the Spike-Triggered Sampling scheme (bottom row). This choice is mathematically motivated by the local reset property of the Galves-Löcherbach dynamics: by anchoring the observation windows to the spikes of the target neuron, the membrane potential is sampled from a known state. This

conditioning significantly reduces the estimator’s variance and enhances the statistical resolvability of the synaptic jump from the contributions of the rest of the network. Consequently, we focus on the two approaches in the second row: the single-scale spike-triggered estimator, which provides a rigorous benchmark under minimal assumptions, and the Macro-Micro Extrapolation, which leverages the regularity of statistical observables across different scales. The latter employs an adaptive hybrid logic—switching between mid-point averaging and pyramid extrapolation—to allow for an intercept recovery toward the micro-scale limit even when direct measurements are dominated by sparsity.

It is also important to note that recent models have been designed to better integrate biological neuronal behavior, such as axonal conduction delays and membrane potential leakage (see, e.g., [2]). The methodologies described in this work are designed to be effective beyond the specific cases presented here; preliminary tests on the model proposed in [2] already suggest that the adaptive extrapolation logic maintains its robustness even in the presence of more complex membrane dynamics and non-zero transmission latencies. Furthermore, the Galves-Löcherbach stochastic model has also been applied to social networks (see [6, 11]) to model fast consensus and metastability in polarized networks, highlighting the relevance of this model in various contexts.

The article is organized as follows. In Section 2, we define the stochastic neural model based on the Galves-Löcherbach framework. Section 3 introduces the core of our methodological shift: the Spike-Triggered Estimator, highlighting its advantages over traditional fixed-grid sampling. In Section 4, we derive the statistical properties of the estimator. Section 5 provides rigorous bounds on the conditional probabilities related to our estimators. We also analytically identify a critical window width (Δ_A) required for single-scale identification, noting that such a resolution is often too fine for practical computational applications. Section 6 is dedicated to sample complexity and the derivation of error bounds. Section 7 provides numerical validation of the single-scale estimator, confirming the theoretical predictions. Section 8 introduces the Macro-Micro Strategy and the Pyramid Extrapolation logic to overcome the limitations of the ultra-fine sampling window. Section 9 stresses the framework under extreme noise conditions using a minimal architecture. Section 10 demonstrates its scalability and robustness in fully interactive and layered networks up to $N = 60$. Section 11 summarizes our findings and outlines future research directions.

2 The Continuous-Time Galves-Löcherbach Model

Having defined the general scope of our inference framework, we now establish the formal mathematical environment by describing the stochastic dynamics of the neuronal network. Following the framework of [10], we model the neural network as a family of interacting point processes ($N^i, i \in I$) defined on a common probability space $(\Omega, \mathcal{F}, \mathbb{P})$, where I is a finite set of neurons. For each neuron $i \in I$, N^i is a random counting measure on $(\mathbb{R}_+, \mathcal{B}(\mathbb{R}_+))$.

For any interval $A = (s, t] \subset \mathbb{R}_+$, $N^i(A)$ represents the number of spikes emitted by neuron i during the time interval A . We assume that the processes are simple, meaning that $\mathbb{P}(N^i(\{t\}) \leq 1 \text{ for all } t \geq 0) = 1$. The sequence of spike times $(T_k^i)_{k \geq 1}$ for neuron i is defined as:

$$T_k^i = \inf\{t > T_{k-1}^i : N^i((T_{k-1}^i, t]) = 1\}. \quad (1)$$

The process N^i can be expressed as $N^i(A) = \sum_{k=1}^{\infty} \mathbf{1}_A(T_k^i)$. For each neuron $i \in I$, the *firing*

intensity $\lambda_i(t)$ is given by:

$$\lambda_i(t) = \phi_i(u_i(t)), \quad (2)$$

where $u_i(t)$ represents the *membrane potential* and $\phi_i : \mathbb{R} \rightarrow \mathbb{R}_+$ is a non-negative, non-decreasing function.

The interaction between neurons is mediated by synaptic weights $w^{j \rightarrow i}$. For each neuron $i \in I$, we denote its **pre-synaptic neighborhood** as $\mathcal{V}^i := \{j \in I : w^{j \rightarrow i} \neq 0\}$, partitioned into the excitatory subset \mathcal{V}_+^i ($w^{j \rightarrow i} > 0$) and the inhibitory subset \mathcal{V}_-^i ($w^{j \rightarrow i} < 0$). We assume a maximum in-degree d , such that $|\mathcal{V}^i| \leq d$.

The system of membrane potentials $\mathbf{u}(t) = (u_i(t))_{i \in I}$ defines the state space of the network. By accounting for the current potentials, the dynamics satisfy the Markov property. For any $t \geq 0$, the potential of neuron i is uniquely determined by the initial state $\mathbf{u}(0)$ and the subsequent spikes:

$$u_i(t) = u_i(0) \mathbf{1}_{\{N^i([0,t])=0\}} + \sum_{j \in \mathcal{V}^i} w^{j \rightarrow i} N^j((L_i(t) \vee 0, t)), \quad (3)$$

where $L_i(t) = \sup\{s < t : N^i(\{s\}) = 1\}$ tracks the most recent reset (with $\sup \emptyset = 0$). Whenever neuron i spikes, its potential $u_i(t)$ is reset to zero, effectively erasing the influence of its previous history.

This Markovian formulation is particularly advantageous for our **Spike-Triggered** approach: by anchoring our observation windows to the spikes of neuron i , we perform a sampling of the Markov chain at the exact moment the potential u_i is known to be zero.

To formalize the information flow, we introduce two filtrations. Let \mathcal{F}_t be the σ -algebra representing the full state of the system up to time t . Conversely, let $\mathcal{H}_t \subset \mathcal{F}_t$ be the σ -algebra generated exclusively by the observable spike trains up to time t .

Remark 1. *By the tower property of conditional expectation, any spiking event E_t relates to the observable history as:*

$$\mathbb{P}(E_t | \mathcal{H}_t) = \mathbb{E}[\mathbb{P}(E_t | \mathcal{F}_t) | \mathcal{H}_t].$$

In the Galves-Löcherbach model, the reset mechanism ensures that conditioning on \mathcal{H}_t effectively captures the information necessary to describe the system's dynamics.

Following [1], we assume:

Assumption 1. *The firing intensity functions $\phi_i : \mathbb{R} \rightarrow \mathbb{R}_+$ satisfy:*

1. non-decreasing;
2. bounded away from 0: $\min_{i \in I} \inf_{u \in \mathbb{R}} \phi_i(u) \geq \alpha > 0$;
3. bounded from above: $\max_{i \in I} \sup_{u \in \mathbb{R}} \phi_i(u) \leq \beta < +\infty$;
4. minimum synaptic jump: $\min_{j \in \mathcal{V}^i} |\phi_i(w^{j \rightarrow i}) - \phi_i(0)| \geq \delta, \quad \forall i \in I$;
5. maximum in-degree: $\max_{i \in I} |\mathcal{V}^i| \leq d$.

We assume that $\alpha, \beta, \delta \in \mathbb{R}^+$ and $d \in \mathbb{N}$ are fixed, known values.

Finally, to establish a benchmark for our inference, we partition the observation period into disjoint blocks of duration 3Δ . For any $k \in \mathbb{N}$ and neurons $i \neq j$, we define the **Fixed Scheme** events:

$$A_k^i(\Delta) = \{N^i((3k-3)\Delta, (3k-2)\Delta] > 0\} \quad (4)$$

$$B_k^i(\Delta) = A_k^i(\Delta) \cap \{N^i((3k-2)\Delta, (3k-1)\Delta] > 0\} \quad (5)$$

$$C_k^{j \rightarrow i}(\Delta) = A_k^i(\Delta) \cap \{N^j((3k-2)\Delta, (3k-1)\Delta] > 0\} \quad (6)$$

$$D_k^{j \rightarrow i}(\Delta) = C_k^{j \rightarrow i}(\Delta) \cap \{N^i((3k-1)\Delta, 3k\Delta] > 0\} \quad (7)$$

In this framework, B_k^i is the *bursting* event, $C_k^{j \rightarrow i}$ the *trigger* event, and $D_k^{j \rightarrow i}$ the *interaction* event.

3 Spike-Triggered Sampling Scheme

In the following, we denote by $A_k^i, B_k^i, C_k^{j \rightarrow i}, D_k^{j \rightarrow i}$ the events associated with the Fixed Scheme, where the index k refers to disjoint temporal blocks of fixed duration. Conversely, we employ the calligraphic notation $\mathcal{A}_k^i, \mathcal{B}_k^i, \mathcal{C}_k^{j \rightarrow i}, \mathcal{D}_k^{j \rightarrow i}$ for the **Spike-Triggered Scheme** introduced in this section. In this framework, the index k refers to two sequences of stopping times $(\tau_k^i)_{k \in \mathbb{N}}$ and $(\sigma_k^{j \rightarrow i})_{k \in \mathbb{N}}$ derived from the firing history of the neurons i and j . These stopping times serve as **dynamic triggers** for the observation windows, allowing for a recursive definition of the sampling events that exploits the local reset property.

3.1 Baseline Triggered Scheme for \mathcal{A}^i and \mathcal{B}^i

Let $(T_j^i)_{j \geq 1}$ be the ordered sequence of spike times of neuron i . We define a sequence of **trigger times** $\{\tau_k^i\}_{k \geq 1}$ and the corresponding sampled events through the following recursive design:

1. **Initialization:**

$$\tau_1^i := T_1^i. \quad (8)$$

2. **Definition of Triggered Events:** For each trigger τ_k^i , we define:
 - The *reference event* \mathcal{A}_k^i , marking the reset of the membrane potential:

$$\mathcal{A}_k^i := \{N^i(\{\tau_k^i\}) = 1\}. \quad (9)$$

- The *bursting event* $\mathcal{B}_k^i(\Delta)$, occurring if neuron i emits at least one subsequent spike within the window $(\tau_k^i, \tau_k^i + \Delta]$:

$$\mathcal{B}_k^i(\Delta) := \{N^i(\tau_k^i, \tau_k^i + \Delta] > 0\}. \quad (10)$$

3. **Conditional Recursive Update:** The next trigger time τ_{k+1}^i is determined by the outcome of $\mathcal{B}_k^i(\Delta)$:
 - **If $\mathcal{B}_k^i(\Delta)$ occurs:** Let $T_{k,burst}^i$ be the first spike in $(\tau_k^i, \tau_k^i + \Delta]$. To preserve the reset condition for the next trial, we skip this spike and set:

$$\tau_{k+1}^i := \inf\{T_\ell^i : T_\ell^i > T_{k,burst}^i\}. \quad (11)$$

- **If $\mathcal{B}_k^i(\Delta)$ does not occur:** The next trigger is the first spike occurring after the current horizon Δ :

$$\tau_{k+1}^i := \inf\{T_\ell^i : T_\ell^i > \tau_k^i + \Delta\}. \quad (12)$$

3.2 Interaction Triggered Scheme for $\mathcal{C}^{j \rightarrow i}$ and $\mathcal{D}^{j \rightarrow i}$

We define a sequence of trigger times $(\sigma_k^{j \rightarrow i})_{k \geq 1}$ dedicated to the interaction analysis, where each trigger coincides with a spike of the target neuron i .

1. **Initialization and Reset:** The first interaction trigger is $\sigma_1^{j \rightarrow i} := T_1^i$. At this instant, the membrane potential u_i is reset to zero, providing a controlled state for the trial.
2. **Causal Triggering (Detection of j):** For each $\sigma_k^{j \rightarrow i}$, we search for the first spike of neuron j after the trigger:

$$T_{k,*}^j := \inf\{T_h^j : T_h^j > \sigma_k^{j \rightarrow i}\}. \quad (13)$$

The **trigger event** $\mathcal{C}_k^{j \rightarrow i}(\Delta)$ is satisfied if this spike falls within the window:

$$\mathcal{C}_k^{j \rightarrow i}(\Delta) := \{T_{k,*}^j \leq \sigma_k^{j \rightarrow i} + \Delta\}. \quad (14)$$

3. **Conditional Observation of $\mathcal{D}_k^{j \rightarrow i}(\Delta)$:** If $\mathcal{C}_k^{j \rightarrow i}(\Delta)$ occurs, a secondary window of length Δ is opened at $T_{k,*}^j$. The *interaction success* occurs if neuron i fires:

$$\mathcal{D}_k^{j \rightarrow i}(\Delta) := \mathcal{C}_k^{j \rightarrow i}(\Delta) \cap \{N^i(T_{k,*}^j, T_{k,*}^j + \Delta) > 0\}. \quad (15)$$

4. **Recursive Update Rule:** The next trigger $\sigma_{k+1}^{j \rightarrow i}$ is determined as follows:

- **If $\mathcal{C}_k^{j \rightarrow i}(\Delta)$ is not satisfied:** The trial is aborted and the next trigger is:

$$\sigma_{k+1}^{j \rightarrow i} := \inf\{T_\ell^i : T_\ell^i > \sigma_k^{j \rightarrow i} + \Delta\}. \quad (16)$$

- **If $\mathcal{C}_k^{j \rightarrow i}(\Delta)$ is satisfied:**

- *Case Success ($\mathcal{D}_k^{j \rightarrow i}(\Delta)$ occurs):* Let $T_{k,\text{react}}^i = \inf\{T_\ell^i : T_\ell^i > T_{k,*}^j\}$. We skip this reaction spike and set:

$$\sigma_{k+1}^{j \rightarrow i} := \inf\{T_\ell^i : T_\ell^i > T_{k,\text{react}}^i\}. \quad (17)$$

- *Case Failure ($\mathcal{D}_k^{j \rightarrow i}(\Delta)$ does not occur):* The next trigger is:

$$\sigma_{k+1}^{j \rightarrow i} := \inf\{T_\ell^i : T_\ell^i > T_{k,*}^j + \Delta\}. \quad (18)$$

The sequence $(\sigma_k^{j \rightarrow i})_{k \geq 1}$ consists of stopping times with respect to the filtration $(\mathcal{F}_t)_{t \geq 0}$. Crucially, by choosing each trigger to coincide with a spike of the target neuron i , the membrane potential $u_i(t)$ is reset at the start of each trial. This local reset mechanism ensures that trials are decoupled, providing the probabilistic foundation required to apply concentration inequalities for the Spike-Triggered Estimator.

4 The Estimators $\hat{G}^{j \rightarrow i}(\Delta)$ and $\hat{\mathcal{G}}^{j \rightarrow i}(\Delta)$

The sampling protocols described in Section 3 allow for the construction of rescaled statistics designed to isolate the functional influence between neurons using pairwise observations. For a given pair of neurons (j, i) , the **Fixed Scheme Estimator** is defined as:

$$\hat{G}_{m_0, m_1}^{j \rightarrow i}(\Delta) := \frac{1}{\Delta \delta} \left(\frac{\sum_{k=1}^{m_1} \mathbf{1}_{D_k^{j \rightarrow i}(\Delta)}}{\sum_{k=1}^{m_1} \mathbf{1}_{C_k^{j \rightarrow i}(\Delta)}} - \frac{\sum_{k=1}^{m_0} \mathbf{1}_{B_k^i(\Delta)}}{\sum_{k=1}^{m_0} \mathbf{1}_{A_k^i(\Delta)}} \right), \quad (19)$$

whereas the **Spike-Triggered Estimator** is defined as:

$$\hat{\mathcal{G}}_{m_0, m_1}^{j \rightarrow i}(\Delta) := \frac{1}{\Delta \delta} \left(\frac{\sum_{k=1}^{m_1} \mathbf{1}_{D_k^{j \rightarrow i}(\Delta)}}{\sum_{k=1}^{m_1} \mathbf{1}_{C_k^{j \rightarrow i}(\Delta)}} - \frac{\sum_{k=1}^{m_0} \mathbf{1}_{B_k^i(\Delta)}}{m_0} \right). \quad (20)$$

4.1 Conditional Probabilities and Ergodic Means

We define the theoretical quantities for a representative trial ($k = 1$), which depend on the specific realization of the history up to the trigger times. For the Fixed Scheme, the theoretical random variable is given by:

$$G^{j \rightarrow i}(\Delta, \mathcal{F}_{\sigma_1^{j \rightarrow i}}, \mathcal{F}'_{\tau_1^i}) := \frac{1}{\Delta \delta} \left[\frac{\mathbb{P}(D_1^{j \rightarrow i}(\Delta) \mid \mathcal{F}_{\sigma_1^{j \rightarrow i}})}{\mathbb{P}(C_1^{j \rightarrow i}(\Delta) \mid \mathcal{F}_{\sigma_1^{j \rightarrow i}})} - \frac{\mathbb{P}(B_1^i(\Delta) \mid \mathcal{F}'_{\tau_1^i})}{\mathbb{P}(A_1^i(\Delta) \mid \mathcal{F}'_{\tau_1^i})} \right], \quad (21)$$

and analogously, for the **Spike-Triggered** approach:

$$\mathcal{G}^{j \rightarrow i}(\Delta, \mathcal{F}_{\sigma_1^{j \rightarrow i}}, \mathcal{F}'_{\tau_1^i}) := \frac{1}{\Delta \delta} \left[\frac{\mathbb{P}(D_1^{j \rightarrow i}(\Delta) \mid \mathcal{F}_{\sigma_1^{j \rightarrow i}})}{\mathbb{P}(C_1^{j \rightarrow i}(\Delta) \mid \mathcal{F}_{\sigma_1^{j \rightarrow i}})} - \frac{\mathbb{P}(B_1^i(\Delta) \mid \mathcal{F}'_{\tau_1^i})}{1} \right]. \quad (22)$$

In these expressions, the interaction term is conditioned on the history \mathcal{F} at the trigger time $\sigma_1^{j \rightarrow i}$, while the baseline term is conditioned on the history \mathcal{F}' at the trigger time τ_1^i .

Under the invariant measures μ and ν (corresponding to fixed and spike-triggered sampling, respectively), the expected values are:

$$G^{j \rightarrow i}(\Delta) := \mathbb{E}_\mu[G^{j \rightarrow i}(\Delta, \mathcal{F}, \mathcal{F}')], \quad (23)$$

$$\mathcal{G}^{j \rightarrow i}(\Delta) := \mathbb{E}_\nu[\mathcal{G}^{j \rightarrow i}(\Delta, \mathcal{F}, \mathcal{F}')]. \quad (24)$$

By ergodicity—which holds for this class of processes under Assumption 1, as proven in [10]—the empirical estimators converge almost surely to their respective ergodic means:

$$\hat{G}_{m_0, m_1}^{j \rightarrow i}(\Delta) \xrightarrow[m_0, m_1 \rightarrow \infty]{\text{a.s.}} G^{j \rightarrow i}(\Delta), \quad \hat{\mathcal{G}}_{m_0, m_1}^{j \rightarrow i}(\Delta) \xrightarrow[m_0, m_1 \rightarrow \infty]{\text{a.s.}} \mathcal{G}^{j \rightarrow i}(\Delta). \quad (25)$$

5 Probabilistic Bounds

We study the range of values that the random variable $\mathbb{P}(B_k^i(\Delta) \mid \mathcal{F}_{\tau_k^i})$ can take, based on the history of the process up to the stopping time τ_k^i .

Lemma 1 (Baseline Probability Estimates). *Under Assumption 1, for any trigger time τ_k^i , the random variable $\mathbb{P}(\mathcal{B}_k^i(\Delta) \mid \mathcal{F}_{\tau_k^i})$ satisfies the following inequalities almost surely:*

$$(1 - e^{-\phi_i(0)\Delta})e^{-\beta|\mathcal{V}^i|\Delta} \leq \mathbb{P}(\mathcal{B}_k^i(\Delta) \mid \mathcal{F}_{\tau_k^i}) \leq (1 - e^{-\phi_i(0)\Delta})e^{-\alpha|\mathcal{V}^i|\Delta} + (1 - e^{-\beta\Delta})(1 - e^{-\beta|\mathcal{V}^i|\Delta}). \quad (26)$$

Proof. Recalling from Section 3, the event $\mathcal{B}_k^i(\Delta)$ represents neuron i emitting at least one spike in the interval $(\tau_k^i, \tau_k^i + \Delta]$. Since the probabilities are conditioned with respect to $\mathcal{F}_{\tau_k^i}$, all subsequent inequalities hold almost surely (\mathbb{P} -a.s.).

By the reset property of the model, $u_i(\tau_k^i) = 0$ a.s.; hence, the firing intensity at the beginning of the interval is $\lambda_i(\tau_k^i) = \phi_i(0)$.

To derive the lower bound, let $N^{\mathcal{V}^i}(\tau_k^i, \tau_k^i + \Delta]$ be the point process representing the spikes of all pre-synaptic neurons $j \in \mathcal{V}^i$. We introduce a dominating Poisson process P^* with constant intensity $\beta|\mathcal{V}^i|$. The following inequalities hold:

$$\begin{aligned} \mathbb{P}(\mathcal{B}_k^i(\Delta) \mid \mathcal{F}_{\tau_k^i}) &\geq \mathbb{P}(\mathcal{B}_k^i(\Delta) \cap \{N^{\mathcal{V}^i}(\tau_k^i, \tau_k^i + \Delta] = 0\} \mid \mathcal{F}_{\tau_k^i}) \\ &\geq \mathbb{P}(\mathcal{B}_k^i(\Delta) \cap \{P^*(\tau_k^i, \tau_k^i + \Delta] = 0\} \mid \mathcal{F}_{\tau_k^i}) \\ &= (1 - e^{-\phi_i(0)\Delta})e^{-\beta|\mathcal{V}^i|\Delta}, \end{aligned} \quad (27)$$

where the second inequality follows from the stochastic dominance of P^* over $N^{\mathcal{V}^i}$.

For the upper bound, we partition the event $\mathcal{B}_k^i(\Delta)$ according to the activity of $N^{\mathcal{V}^i}(\tau_k^i, \tau_k^i + \Delta]$. Using a dominated Poisson process P_* (intensity $\alpha|\mathcal{V}^i|$) and the dominating process P^* , we obtain

$$\begin{aligned} \mathbb{P}(\mathcal{B}_k^i(\Delta) \mid \mathcal{F}_{\tau_k^i}) &\leq \\ &\mathbb{P}(\mathcal{B}_k^i(\Delta) \cap \{N^{\mathcal{V}^i}(\tau_k^i, \tau_k^i + \Delta] = 0\} \mid \mathcal{F}_{\tau_k^i}) + \mathbb{P}(\mathcal{B}_k^i(\Delta) \cap \{N^{\mathcal{V}^i}(\tau_k^i, \tau_k^i + \Delta] > 0\} \mid \mathcal{F}_{\tau_k^i}) \\ &\mathbb{P}(\mathcal{B}_k^i(\Delta) \cap \{P_*(\tau_k^i, \tau_k^i + \Delta] = 0\} \mid \mathcal{F}_{\tau_k^i}) + \mathbb{P}(\mathcal{B}_k^i(\Delta) \cap \{P^*(\tau_k^i, \tau_k^i + \Delta] > 0\} \mid \mathcal{F}_{\tau_k^i}) \\ &\leq (1 - e^{-\phi_i(0)\Delta})e^{-\alpha|\mathcal{V}^i|\Delta} + (1 - e^{-\beta\Delta})(1 - e^{-\beta|\mathcal{V}^i|\Delta}) \end{aligned} \quad (28)$$

In (28), the second term is bounded by setting the firing intensity to β for neuron i whenever the neighborhood is active. \square

As stated in (26), the probabilistic bounds can be simplified via Taylor expansion using the Lagrange form of the remainder. For any $x \geq 0$:

$$1 - x \leq e^{-x} \leq 1 - x + \frac{x^2}{2}. \quad (29)$$

By combining Lemma 1, (29) with the assumption that $|\mathcal{V}^i| \leq d$, we obtain

Corollary 1. *Under the same assumptions as Lemma 1,*

$$\phi_i(0)\Delta - \left(d + \frac{1}{2}\right)\beta^2\Delta^2 \leq \mathbb{P}(\mathcal{B}_k^i(\Delta) \mid \mathcal{F}_{\tau_k^i}) \leq \phi_i(0)\Delta + d\beta^2\Delta^2. \quad (30)$$

Lemma 2 quantifies the modulation of the bursting probability induced by a pre-synaptic event from neuron j .

Lemma 2 (Probability Ratios for Connectivity). *Let $\Delta > 0$. For any target neuron i and candidate pre-synaptic neuron j , the conditional probability of an interaction success satisfies the following bounds P -a.s.:*

1. **No Connection** ($j \notin \mathcal{V}^i$):

$$(1 - e^{-\phi_i(0)\Delta})e^{-2|\mathcal{V}^i|\beta\Delta} \leq \frac{\mathbb{P}(\mathcal{D}_k^{j \rightarrow i}(\Delta) \mid \mathcal{F}_{\sigma_k^i})}{\mathbb{P}(\mathcal{C}_k^{j \rightarrow i}(\Delta) \mid \mathcal{F}_{\sigma_k^i})} \leq (1 - e^{-\phi_i(0)\Delta}) + (1 - e^{-\beta\Delta})(1 - e^{-2\beta|\mathcal{V}^i|\Delta}) \quad (31)$$

2. **Excitatory Connection** ($j \in \mathcal{V}_+^i$):

$$\frac{\mathbb{P}(\mathcal{D}_k^{j \rightarrow i}(\Delta) \mid \mathcal{F}_{\sigma_k^i})}{\mathbb{P}(\mathcal{C}_k^{j \rightarrow i}(\Delta) \mid \mathcal{F}_{\sigma_k^i})} \geq (1 - e^{-(\phi_i(0)+\delta)\Delta})e^{-2\beta(|\mathcal{V}^i|-1)\Delta} \quad (32)$$

3. **Inhibitory Connection** ($j \in \mathcal{V}_-^i$):

$$\frac{\mathbb{P}(\mathcal{D}_k^{j \rightarrow i}(\Delta) \mid \mathcal{F}_{\sigma_k^i})}{\mathbb{P}(\mathcal{C}_k^{j \rightarrow i}(\Delta) \mid \mathcal{F}_{\sigma_k^i})} \leq (1 - e^{-(\phi_i(0)-\delta)\Delta}) + (1 - e^{-\beta\Delta})(1 - e^{-2\beta(|\mathcal{V}^i|-1)\Delta}) \quad (33)$$

Proof. Since $\mathcal{D}_k^{j \rightarrow i}(\Delta) \subseteq \mathcal{C}_k^{j \rightarrow i}(\Delta)$, the ratio becomes

$$\frac{\mathbb{P}(\mathcal{D}_k^{j \rightarrow i}(\Delta) \mid \mathcal{F}_{\sigma_k^i})}{\mathbb{P}(\mathcal{C}_k^{j \rightarrow i}(\Delta) \mid \mathcal{F}_{\sigma_k^i})} = \mathbb{P}(\mathcal{D}_k^{j \rightarrow i}(\Delta) \mid \mathcal{C}_k^{j \rightarrow i}(\Delta), \mathcal{F}_{\sigma_k^i}). \quad (34)$$

Recalling the definition in (13), let

$$\mathbb{P}(\mathcal{D}_k^{j \rightarrow i}(\Delta) \mid T_{k,*}^j = t_*, \mathcal{F}_{\sigma_k^i}), \quad \text{for } t_* \in (\sigma_k^i, \sigma_k^i + \Delta). \quad (35)$$

Lower bound $j \notin \mathcal{V}^i$. Let $\mathcal{E}_k^{j \rightarrow i}(t_*)$ be the event where all pre-synaptic neurons in \mathcal{V}^i remain silent in $(\sigma_k^i, t_* + \Delta]$. Using a dominating Poisson process P^* with intensity $\beta|\mathcal{V}^i|$, the following holds:

$$\begin{aligned} \mathbb{P}(\mathcal{D}_k^{j \rightarrow i}(\Delta) \mid T_{k,*}^j = t_*, \mathcal{F}_{\sigma_k^i}) &\geq \mathbb{P}(\mathcal{D}_k^{j \rightarrow i}(\Delta) \cap \mathcal{E}_k^{j \rightarrow i}(t_*) \mid T_{k,*}^j = t_*, \mathcal{F}_{\sigma_k^i}) \\ &\geq \mathbb{P}(\mathcal{D}_k^{j \rightarrow i}(\Delta) \cap \{P^*(\sigma_k^i, t_* + \Delta] = 0\} \mid T_{k,*}^j = t_*, \mathcal{F}_{\sigma_k^i}) \\ &\geq (1 - e^{-\phi_i(0)\Delta})e^{-2\beta|\mathcal{V}^i|\Delta}. \end{aligned} \quad (36)$$

Upper bound $j \notin \mathcal{V}^i$. Decomposing $\mathcal{D}_k^{j \rightarrow i}(\Delta)$ via $\mathcal{E}_k^{j \rightarrow i}(t_*)$ and its complement:

$$\begin{aligned} \mathbb{P}(\mathcal{D}_k^{j \rightarrow i}(\Delta) \mid T_{k,*}^j = t_*, \mathcal{F}_{\sigma_k^i}) &\leq \mathbb{P}(\mathcal{D}_k^{j \rightarrow i}(\Delta) \mid \mathcal{E}_k^{j \rightarrow i}(t_*), T_{k,*}^j = t_*, \mathcal{F}_{\sigma_k^i}) \\ &\quad + \mathbb{P}(\mathcal{D}_k^{j \rightarrow i}(\Delta) \cap (\mathcal{E}_k^{j \rightarrow i}(t_*))^c \mid T_{k,*}^j = t_*, \mathcal{F}_{\sigma_k^i}). \end{aligned} \quad (37)$$

Under $\mathcal{E}_k^{j \rightarrow i}(t_*)$, with $j \notin \mathcal{V}^i$, the intensity λ_i equals $\phi_i(0)$. For the second term, independent dominating Poisson processes P^* (intensity $d\beta$) and P^{**} (intensity β) yield:

$$\begin{aligned} \mathbb{P}(\mathcal{D}_k^{j \rightarrow i}(\Delta) \mid T_{k,*}^j = t_*, \mathcal{F}_{\sigma_k^i}) &\leq (1 - e^{-\phi_i(0)\Delta}) + \mathbb{P}(P^{**}(\Delta) \geq 1) \cdot \mathbb{P}(P^*(2\Delta) \geq 1) \\ &= (1 - e^{-\phi_i(0)\Delta}) + (1 - e^{-\beta\Delta})(1 - e^{-2\beta|\mathcal{V}^i|\Delta}). \end{aligned} \quad (38)$$

Excitatory Connection $j \in \mathcal{V}_+^i$. After the firing of neuron j , the intensity of neuron i satisfies $\lambda_i \geq \phi_i(0) + \delta$. Using $|\mathcal{V}^i| - 1$ in the exponent to account for the neighborhood excluding j , and applying Assumption 1 (non-decreasing ϕ_i), the bound (32) follows.

Inhibitory Connection $j \in \mathcal{V}_-^i$. The argument follows analogously by applying the lower bound of the firing intensity, $\phi_i(0) - \delta$, and following the same steps as in the excitatory case. \square

5.1 Explicit Linear-Quadratic Bounds

Following the results established in Lemma 2, we simplify the exponential bounds into a more manageable linear-quadratic form. By utilizing a Taylor expansion with a Lagrange remainder and $|\mathcal{V}^i| \leq d$, we obtain

Corollary 2. *Under the assumptions of Lemma 2, the ratio of conditional probabilities for any pair of neurons (j, i) satisfies the following explicit bounds almost surely (P -a.s.):*

1. **No Connection** ($j \notin \mathcal{V}^i$):

$$\phi_i(0)\Delta - \left(2d + \frac{1}{2}\right)\beta^2\Delta^2 \leq \frac{\mathbb{P}(\mathcal{D}_k^{j \rightarrow i}(\Delta)|\mathcal{F}_{\sigma_k^i})}{\mathbb{P}(\mathcal{C}_k^{j \rightarrow i}(\Delta)|\mathcal{F}_{\sigma_k^i})} \leq \phi_i(0)\Delta + 2d\beta^2\Delta^2 \quad (39)$$

2. **Excitatory Connection** ($j \in \mathcal{V}_+^i$):

$$\frac{\mathbb{P}(\mathcal{D}_k^{j \rightarrow i}(\Delta)|\mathcal{F}_{\sigma_k^i})}{\mathbb{P}(\mathcal{C}_k^{j \rightarrow i}(\Delta)|\mathcal{F}_{\sigma_k^i})} \geq (\phi_i(0) + \delta)\Delta - \left(2d - \frac{1}{2}\right)\beta^2\Delta^2 \quad (40)$$

3. **Inhibitory Connection** ($j \in \mathcal{V}_-^i$):

$$\frac{\mathbb{P}(\mathcal{D}_k^{j \rightarrow i}(\Delta)|\mathcal{F}_{\sigma_k^i})}{\mathbb{P}(\mathcal{C}_k^{j \rightarrow i}(\Delta)|\mathcal{F}_{\sigma_k^i})} \leq (\phi_i(0) - \delta)\Delta + (2d - 2)\beta^2\Delta^2 \quad (41)$$

Proof. These inequalities are derived by applying (29) to the terms found in Lemma 2.

Specifically, for the **lower bounds** of the form $(1 - e^{-\lambda\Delta})e^{-\gamma\Delta}$, we use:

$$(1 - e^{-\lambda\Delta})e^{-\gamma\Delta} \geq \left(\lambda\Delta - \frac{\lambda^2\Delta^2}{2}\right)(1 - \gamma\Delta) = \lambda\Delta - \left(\lambda\gamma + \frac{\lambda^2}{2}\right)\Delta^2 + \frac{\lambda^2\gamma\Delta^3}{2} \quad (42)$$

By dropping the positive Δ^3 term and substituting the upper bounds $\lambda \leq \beta$ and $\gamma \leq 2d\beta$ (or $2(d-1)\beta$), we obtain the constants $\beta^2(2d + 0.5)$ and $\beta^2(2(d-1) + 0.5)$.

For the **upper bounds**, which involve terms like $(1 - e^{-\lambda\Delta}) + (1 - e^{-\beta\Delta})(1 - e^{-\gamma\Delta})$, we use:

$$(1 - e^{-\lambda\Delta}) + (1 - e^{-\beta\Delta})(1 - e^{-\gamma\Delta}) \leq \lambda\Delta + (\beta\Delta)(\gamma\Delta) = \lambda\Delta + \beta\gamma\Delta^2. \quad (43)$$

Substituting $\gamma = 2d\beta$ (or $2(d-1)\beta$) yields the constants $2d\beta^2$ and $2(d-1)\beta^2$. The validity of these bounds for any $\Delta > 0$ is guaranteed by the Taylor expansion with Lagrange remainder. This justifies the omission of the remainder in the lower and upper bounds, respectively, ensuring the inequalities hold. \square

5.2 Rigorous Bounds for $\mathcal{G}^{j \rightarrow i}(\Delta)$

By combining the results of Corollary 1 and Corollary 2, we derive the formal bounds for the scaled random variable $\mathcal{G}^{j \rightarrow i}(\Delta)$ defined in (20). This quantity isolates the synaptic influence by centering the baseline firing rate and normalizing it by the parameters δ and Δ .

To ensure that the identification of the connectivity is not affected by finite-window effects, we introduce the operational condition:

$$9d\beta^2\Delta \leq \delta. \quad (44)$$

Under this constraint, the gap between the probability ratios for different connection types remains strictly positive and proportional to $\delta\Delta$. This ensures that the quadratic error does not obscure the excitatory or inhibitory signal.

Theorem 1 (Stability of Interaction Estimators). *Under the scaling condition (44), the functions $\mathcal{G}^{j \rightarrow i}(\Delta)$ and $\mathcal{G}^{j \rightarrow i}(\Delta)$ satisfy the following inequalities:*

1. If $j \notin \mathcal{V}^i$, then

$$|\mathcal{G}^{j \rightarrow i}(\Delta)| \leq \frac{(3d + 0.5)\beta^2}{\delta}\Delta. \quad (45)$$

2. If $j \in \mathcal{V}_+^i$, then

$$\mathcal{G}^{j \rightarrow i}(\Delta) \geq 1 - \frac{3d\beta^2}{\delta}\Delta. \quad (46)$$

3. If $j \in \mathcal{V}_-^i$, then

$$\mathcal{G}^{j \rightarrow i}(\Delta) \leq -1 + \frac{\beta^2(3d - 1.5)}{\delta}\Delta. \quad (47)$$

Proof. The bounds are established by substituting the linear-quadratic expansions into the definition of the random interaction strength (22). Note that the ratios represent the conditional probabilities of a spike occurring within a window Δ , given the occurrence of the respective trigger events.

For the excitatory case ($j \in \mathcal{V}_+^i$), applying the estimates from Corollaries 1 and 2, we obtain:

$$\begin{aligned} \Delta\delta\mathcal{G}^{j \rightarrow i}(\Delta, \cdot) &\geq [(\phi_i(0) + \delta)\Delta - \beta^2(2d - 0.5)\Delta^2] - [\phi_i(0)\Delta + d\beta^2\Delta^2] \\ &= \delta\Delta - \beta^2(3d - 0.5)\Delta^2. \end{aligned}$$

Dividing by $\Delta\delta$ yields:

$$\mathcal{G}^{j \rightarrow i}(\Delta, \mathcal{F}_{\sigma_1^{j \rightarrow i}}, \mathcal{F}'_{\tau_1^i}) \geq 1 - \frac{\beta^2(3d - 0.5)}{\delta}\Delta.$$

The uniformity of these bounds with respect to the history $(\mathcal{F}_t)_{t \geq 0}$, guaranteed by the reset property at times $\sigma_k^{j \rightarrow i}$ and τ_k^i , allows us to extend the result to the expected function $\mathcal{G}^{j \rightarrow i}(\Delta)$ via the stationary measure $\mathbb{E}_\nu[\cdot]$. The null and inhibitory cases follow by analogous arguments. \square

These results allow us to establish a statistical criterion for the identification of excitatory, inhibitory, and null connections.

Corollary 3 (Topology Identification). *For an observation window $\Delta_A = \frac{\delta}{9d\beta^2}$, the function $\mathcal{G}^{j \rightarrow i}(\Delta)$ provides an explicit separation of the network topology:*

1. **No Connection** ($j \notin \mathcal{V}^i$):

$$|\mathcal{G}^{j \rightarrow i}(\Delta_A)| \leq \frac{1}{3} + \frac{1}{18d}. \quad (48)$$

2. **Excitatory Connection** ($j \in \mathcal{V}_+^i$):

$$\mathcal{G}^{j \rightarrow i}(\Delta_A) \geq \frac{2}{3}. \quad (49)$$

3. **Inhibitory Connection** ($j \in \mathcal{V}_-^i$):

$$\mathcal{G}^{j \rightarrow i}(\Delta_A) \leq -\frac{2}{3} - \frac{1}{6d}. \quad (50)$$

5.3 Comparison with Previous Identification Bounds

We compare the analytical bounds established in Corollaries 1 and 2 with the results presented in Lemma 3 of [1]. The estimates derived in this work provide a sharper characterization of the interaction function $\mathcal{G}^{j \rightarrow i}(\Delta)$ for the following reasons.

1. Estimator Construction. The estimator in [1] is defined on a fixed-time grid, whereas the current estimator is constructed using the stopping times $(\sigma_k^{j \rightarrow i}, \tau_k^i)$. By the reset property, this construction fixes the initial intensity at $\lambda_i = \phi_i(0)$, removing the dependence on the history of the process for the target neuron i . This leads to sharper analytical bounds and more stable statistics compared to the fixed-grid approach.

2. Analytical Refinement of the Bounds. In Lemma 3 of [1], the error estimates were dependent on the leak rate α . The refined analytical treatment in the current work removes the dependence on α from the denominators, providing a more direct representation of the synaptic interaction.

Comparing the error constants C_{2022} with the constants C_{2026} from Corollaries 1 and 2, we observe a systematic reduction in the error terms. Even assuming $\phi_i(0) = \alpha$, which yields the most favorable estimates for the previous framework, the bounds compare as follows:

1. **Base Firing Ratio**, $\mathbb{P}(\mathcal{B}_k^i(\Delta) | \mathcal{F}_{\tau_k^i})$:

- Lower Bound: $C_{2026} = (d + 0.5)\beta^2$ vs $C_{2022} = 3d\beta^2$
- Upper Bound: $C_{2026} = d\beta^2$ vs $C_{2022} \geq 4d\beta^3/\alpha$

2. **Probability Ratio** $\mathbb{P}(\mathcal{D}_k^{j \rightarrow i}(\Delta) | \mathcal{C}_k^{j \rightarrow i}(\Delta), \mathcal{F}_{\sigma_k^i})$:

- **Excitatory Case** ($j \in \mathcal{V}_+^i$):
 - Lower Bound: $C_{2026} = (2d - 0.5)\beta^2$ vs $C_{2022} \geq 5d\beta^3/\alpha$

- **Inhibitory Case** ($j \in \mathcal{V}_-$):
 - Upper Bound: $C_{2026} = (2d - 2)\beta^2$ vs $C_{2022} \geq 5d\beta^4/\alpha^2$
- **Null Case** ($j \notin \mathcal{V}^i$):
 - Lower Bound: $C_{2026} = (2d + 0.5)\beta^2$ vs $C_{2022} \geq 5d\beta^3/\alpha$
 - Upper Bound: $C_{2026} = 2d\beta^2$ vs $C_{2022} \geq 5d\beta^4/\alpha^2$

5.4 Spike-Triggered Estimator with a Single-Scale Window

The empirical estimator $\hat{\mathcal{G}}_{m_0, m_1}^{j \rightarrow i}(\Delta_A)$ is employed to classify the synaptic interaction between any pair of neurons (j, i) . We define the following Statistical Classifier:

$$\hat{S}_{ij}(m_0, m_1) := \begin{cases} 1 & \text{if } \hat{\mathcal{G}}_{m_0, m_1}^{j \rightarrow i}(\Delta_A) > \frac{1}{2}, \\ -1 & \text{if } \hat{\mathcal{G}}_{m_0, m_1}^{j \rightarrow i}(\Delta_A) < -\frac{1}{2}, \\ 0 & \text{if } |\hat{\mathcal{G}}_{m_0, m_1}^{j \rightarrow i}(\Delta_A)| \leq \frac{1}{2}. \end{cases} \quad (51)$$

By Corollary 3, we obtain that

$$\mathcal{G}^{j \rightarrow i}(\Delta_A) \in \begin{cases} \left(\frac{2}{3}, +\infty\right) \subset \left(\frac{1}{2}, +\infty\right) & \text{if } j \rightarrow i \text{ is excitatory,} \\ \left[-\frac{1}{3} - \frac{1}{18d}, \frac{1}{3} + \frac{1}{18d}\right] \subset \left[-\frac{1}{2}, \frac{1}{2}\right] & \text{if } j \text{ is not pre-synaptic to } i, \\ \left(-\infty, -\frac{2}{3} - \frac{1}{6d}\right] \subset \left(-\infty, -\frac{1}{2}\right) & \text{if } j \rightarrow i \text{ is inhibitory.} \end{cases} \quad (52)$$

By combining (25) and (52), we conclude that the statistical classifier $\hat{S}_{ij}(m_0, m_1)$ is asymptotically correct, ensuring that the probability of an error in the classification vanishes as $m_0, m_1 \rightarrow \infty$. As illustrated in Figure 1, the decision space is partitioned by thresholds $\zeta_{\pm} = \pm 1/2$ into three regions: Excitatory, Null, and Inhibitory one.

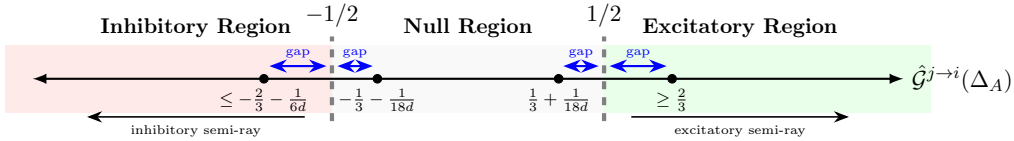


Figure 1: Classification map for topology identification. The decision space is partitioned by thresholds $\zeta_{\pm} = \pm 1/2$. The blue gaps represent the safety margins that accommodate the statistical error of the estimator $\hat{\mathcal{G}}^{j \rightarrow i}(\Delta_A)$, ensuring it remains within the correct decision region relative to the theoretical bounds.

6 Sample Complexity and Robustness Analysis

While Section 5 established the asymptotic correctness of the Spike-Triggered Estimator, we now address its sample complexity. This analysis determines the number of trigger events m_1 required to ensure that the statistical fluctuations of $\hat{\mathcal{G}}^{j \rightarrow i}(\Delta)$ do not cross the decision thresholds defined in (51).

6.1 Variance of the Triggered Statistic

The estimator $\hat{\mathcal{G}}_{m_0, m_1}^{j \rightarrow i}(\Delta)$ is a combination of Bernoulli trials. Crucially, the Spike-Triggered Scheme ensures that trials are decoupled through the reset property. The estimation error is dominated by the interaction term:

$$\hat{\Phi}_{m_1}^{j \rightarrow i}(\Delta) = \frac{\sum_{k=1}^{m_1} \mathbf{1}_{\mathcal{D}_k^{j \rightarrow i}(\Delta)}}{\sum_{k=1}^{m_1} \mathbf{1}_{\mathcal{C}_k^{j \rightarrow i}(\Delta)}}. \quad (53)$$

Let $M = \sum_{k=1}^{m_1} \mathbf{1}_{\mathcal{C}_k^{j \rightarrow i}(\Delta)}$ be the number of "active" trials where neuron j actually fired after the trigger. Since $\mathcal{D}_k \subseteq \mathcal{C}_k$, the term $\hat{\Phi}$ is an empirical mean of M Bernoulli variables with success probability $p \approx \mathbb{P}(\mathcal{D} | \mathcal{C})$.

6.2 Concentration and Sample Complexity

To ensure that the classification \hat{S}_{ij} is correct with high probability $1-q$, we require the deviation $|\hat{\mathcal{G}} - \mathcal{G}|$ to be smaller than the safety gap identified in Figure 1. By applying Bennett's inequality to the decoupled trials, we find that the number of required active trials $M(\Delta)$ scales with the inverse of the signal:

$$M(\Delta) \geq \frac{2 \ln(2/q)}{\sigma^2(\Delta) h(\eta)}, \quad (54)$$

where $\sigma^2(\Delta) \approx p(1-p)$ is the variance. In the small- Δ regime, $p \approx (\phi_i(0) + \delta)\Delta$, making the variance proportional to Δ .

6.3 Total Trigger Requirements

A key result of this work is the calculation of the total sampling effort m_1 . Since the event \mathcal{C} (neuron j firing within Δ after the trigger) occurs with probability $\mathbb{P}(\mathcal{C}) \approx \alpha\Delta$, we must observe many triggers to collect enough active trials M . The total number of triggers m_1 scales as:

$$m_1(\Delta) \approx \frac{M(\Delta)}{\mathbb{P}(\mathcal{C})} = \Theta\left(\frac{1}{\alpha^2 \Delta^2}\right). \quad (55)$$

This quadratic dependence on $(\alpha\Delta)^{-1}$ is the price paid for the high resolution of the continuous-time model.

6.4 Parameter Calibration and Stability

Using the optimal window $\Delta_A = \frac{\delta}{9d\beta^2}$ from Corollary 3, and substituting the dimensionless ratios $s = \alpha/\beta$ and $\tau = \delta/\beta$, the total required trigger events m_1^* is:

$$m_1^* \approx \frac{81d^2 \ln(1/q)}{s^2 \tau^2 h(\eta)} \approx \frac{16200 d^2 \ln(1/q)}{s^2 \tau^4}. \quad (56)$$

This expression highlights that the Spike-Triggered Estimator is particularly sensitive to the synaptic jump τ . However, because the reset mechanism eliminates the history-induced variance (the " α -noise" discussed in Section 5.4), the constant pre-factor is significantly lower than that of the Fixed Scheme, making the identification feasible even with moderate recording lengths.

7 Numerical Validation of the Spike-Triggered Estimator

In this section, we provide a numerical validation of the inference framework. The objective is to verify that the Spike-Triggered Estimator $\hat{\mathcal{G}}_{m_0, m_1}^{j \rightarrow i}$ converges correctly and that the decision thresholds $\zeta = \pm 1/2$ provide a robust separation of the connectivity types under the predicted sample complexity.

7.1 Simulation Setup

We adopt a global activation function $\phi(u)$ for all neurons $i \in I$, defined as the following piecewise linear function:

$$\phi(u) = \begin{cases} \alpha & \text{if } u \leq u_{low}, \\ \beta & \text{if } u \geq u_{high}, \\ \alpha + (u - u_{low}) \frac{\beta - \alpha}{u_{high} - u_{low}} & \text{if } u_{low} < u < u_{high}. \end{cases} \quad (57)$$

For these simulations, we set $\alpha = 1$, $\beta = 5$, $u_{low} = -2.0$, and $u_{high} = 2.0$. This configuration implies $\phi(0) = 3$ (the firing intensity at the reset potential). To validate the classification framework, we select synaptic weights $w^{j \rightarrow i} \in \{1, -1, 0\}$ for excitatory, inhibitory, and null connections, respectively.

The system is composed of N nodes, where Node 0 is the target (post-synaptic) neuron, while the remaining nodes act as independent "driver" nodes (Poisson processes with intensity 3) that exert influence only on Node 0.

7.2 Results and Discussion

The numerical results, summarized in Table 2, confirm that the Spike-Triggered Estimator acts as a reliable topological classifier. In our simulations, we maintained a sparse connectivity with a local in-degree $d = 2$ or $d = 4$.

The results verify a key theoretical intuition: the systematic error (bias) of the estimator depends primarily on the local neighborhood \mathcal{V}^i and the window Δ , rather than the global size N . As long as d remains small, the quadratic interference term $d\beta^2\Delta^2$ remains controlled, and the separation gap between different connection types remains sharp.

The increase in the number of triggers to $N_D = 300$ for the $N = 10$ case was used to ensure robust statistical convergence. The estimates for null links remain consistently near zero ($|\hat{\mathcal{G}}| \approx 0.02$), proving that the estimator correctly ignores "indirect" connections.

While we verified that for $d \leq 5$ the estimator correctly classifies links using window sizes $\Delta \approx \frac{\delta}{\beta^2 d}$, adhering strictly to the ultra-fine resolution Δ_A suggested by the conservative bounds of Corollary 3 poses significant practical limitations. For instance, with $d = 9$, $\Delta_A \approx 0.00049$ would necessitate computationally prohibitive simulation timescales.

For this reason, the single-scale Spike-Triggered approach serves as the foundation for the Macro-Micro methods, which overcome these limitations by investigating the asymptotic behavior of $\hat{\mathcal{G}}^{j \rightarrow i}(\Delta)$ as $\Delta \rightarrow 0^+$, allowing for robust inference even with broader, more practical windows.

Table 2: Classification results for the Spike-Triggered Estimator across different network sizes and window widths.

N	N_D	Link Type	Δ	$\hat{\mathcal{G}}$	Threshold ζ	Outcome
4	100	Excitatory (+1)	0.055	0.8493	± 0.5	✓ Correct
4	100	Null (0.0)	0.055	0.0472	± 0.5	✓ Correct
4	100	Excitatory (+1)	0.009	0.9285	± 0.5	✓ Correct
10	300	Excitatory (+1)	0.009	1.1173	± 0.5	✓ Correct
10	300	Inhibitory (-1)	0.009	-0.8316	± 0.5	✓ Correct
10	300	Null (0.0)	0.009	-0.0276	± 0.5	✓ Correct

8 The Macro-Micro Strategy

The proposed inference framework aims to reconstruct microscopic synaptic connections from observations at macroscopic time scales. This is achieved by evaluating the Spike-Triggered Estimator $\hat{\mathcal{G}}^{j \rightarrow i}$ over a multi-scale temporal grid $\{\Delta_k\}_{k=1}^5$ and employing an adaptive extrapolation-averaging logic to recover the synaptic signal.

8.1 Multi-Scale Calibration

The temporal scales are chosen in a geometric progression $\Delta_k = (\sqrt{2})^{k-1} \Delta_1$. The initial window Δ_1 is analytically determined to ensure the algorithm operates within a statistically significant yet linear regime:

$$\Delta_1 = \underbrace{\frac{1}{\beta d}}_{\text{Noise Scale}} \cdot \underbrace{\frac{\delta}{\beta}}_{\text{Sensitivity}} \cdot \underbrace{\frac{\beta - \alpha}{2\delta}}_{\text{Survival distance}} = \frac{\beta - \alpha}{2d\beta^2}. \quad (58)$$

By exploiting the knowledge of the intensity function $\phi(u)$, this calibration ensures that Δ_1 is large enough to provide signal but small enough to avoid the saturation boundaries of the membrane potential.

8.2 The Extrapolation Models

To decouple the microscopic signal from macroscopic interference, we consider two complementary approaches for analyzing the evolution of $\mathcal{G}(\Delta)$.

1. Local Quadratic Approximation We assume that for small Δ , the gain function follows a second-order expansion:

$$\mathcal{G}^{j \rightarrow i}(\Delta) \approx a\Delta^2 + b\Delta + c, \quad (59)$$

where c represents the direct synaptic effect, $b\Delta$ accounts for first-order interference from other presynaptic neurons, and $a\Delta^2$ aggregates global network noise and non-linearities.

2. Pyramid Extrapolation (P) To avoid the fragility and overfitting risks of direct parabolic fitting, we employ a recursive geometric construction designed for robust intercept recovery. This method, termed **Pyramid Extrapolation**, operates through two phases:

- **Contraction via Barycentric Iteration:** Starting from the multi-scale dataset $\{(\Delta_k, \hat{\mathcal{G}}(\Delta_k))\}_{k=1}^5$, the algorithm computes successive midpoint iterations. This process condenses the five initial samples into two robust “meta-points”, denoted as A and B .
- **Linear Projection and Intercept Recovery:** The final estimate P is defined as the y-intercept of the line passing through meta-points A and B .

The hierarchical structure of the averages captures the *implicit curvature* of the underlying gain function. This provides an intrinsic regularization of the signal, effectively acting as a discrete low-pass filter. It allows the model to track the fundamental trend required for synaptic classification while remaining resilient to high-frequency stochastic fluctuations (outliers) that plague measurements at extremely small scales.

8.3 Hybrid Decision Logic: Pyramid vs. Mean

The core of our strategy lies in the adaptive selection between the Pyramid Extrapolation (P) and the Sample Mean (M) of the gains. Let $\mathcal{S} = \{+1, 0, -1\}$ be the set of theoretical synaptic states. The final index I is chosen via a distance-minimization rule:

$$I = \arg \min_{X \in \{P, M\}} (\text{dist}(X, \mathcal{S})). \quad (60)$$

This hybrid approach balances stability and sensitivity based on the network’s regime:

- **The Mean (M)** is superior in **balanced noise regimes**, where stochastic fluctuations tend to cancel out. It provides a grounded, stable estimate, especially for null ($w = 0$) links.
- **The Pyramid (P)** is essential in **unbalanced regimes** (e.g., predominantly excitatory drive). The background activity biases the gains; the pyramid effectively “strips away” this background slope, allowing the true micro-scale intercept to emerge.

8.4 Classification

To prioritize the suppression of false positives, we adopt a conservative thresholding logic with an explicit safety buffer:

$$\hat{\Sigma}_{ij} = \begin{cases} 1 & \text{if } I > 5/8, \\ -1 & \text{if } I < -5/8, \\ 0 & \text{if } |I| \leq 5/8. \end{cases} \quad (61)$$

While a symmetric threshold at $\pm 1/2$ would be theoretically sufficient, the expansion of the null region to $\pm 5/8$ ensures that residual stochastic fluctuations in larger networks do not trigger misclassifications.

9 Numerical Validation for Macro-Micro Extrapolation

To validate the robustness of our framework under extreme conditions, we consider a target neuron ($i = 0$) influenced by three presynaptic units. Neuron 1 maintains a constant intensity

$\frac{\alpha+\beta}{2}$, while Neurons 2 and 3 aggregate the activity of excitatory (L_+) and inhibitory (L_-) populations, respectively.

This simplified architecture, illustrated in Fig. 2, provides a controlled environment to stress the framework under conditions of extremely low Signal-to-Noise Ratio (SNR). By setting $L_+, L_- \gg \beta$, we simulate a dominant stochastic background drive that would typically obscure synaptic signals in standard observation windows.

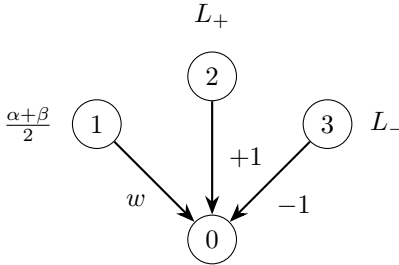


Figure 2: Minimal network architecture for validation.

Computational Advantages of the Minimal Network Architecture

The selection of this topology offers significant advantages for event-driven simulations using Lewis’ thinning algorithm:

1. **Reduced State Update Overhead:** Since the intensity functions follow predictable trajectories between spikes, the calculation of λ_{max} becomes computationally trivial, minimizing the overhead of variable tracking.
2. **Efficiency in Event Attribution:** In this 4-neuron configuration, the search for the triggered unit among candidate spikes requires evaluating only four probabilities, ensuring that the computational cost per event remains extremely low.
3. **Immediate Realization of the Reset State:** By assuming an initial state $u = 0$ for the target neuron, we bypass the initial transient phases. Since presynaptic inputs are independent Poisson processes, the system is natively in statistical equilibrium, providing immediate access to post-reset dynamics.

Experimental Framework and Results

We conducted a systematic campaign of 810 independent simulations across 27 operational scenarios, defined by the interplay of α , β , the load configurations L_{\pm} , and the weights w of Neuron 1.

The empirical results highlight the practical effectiveness of the **Pyramid Extrapolation**. In all 810 trials, the model consistently achieved correct classification. Even in the most extreme regime ($\beta = 7$, aggregate noise of 400 Hz), the iterative averaging effectively isolates the synaptic sign.

As illustrated in Figure 3, the stability of the recovered intercepts (0.964 for excitatory, -1.045 for inhibitory) suggests that this heuristic extrapolation effectively absorbs the bias

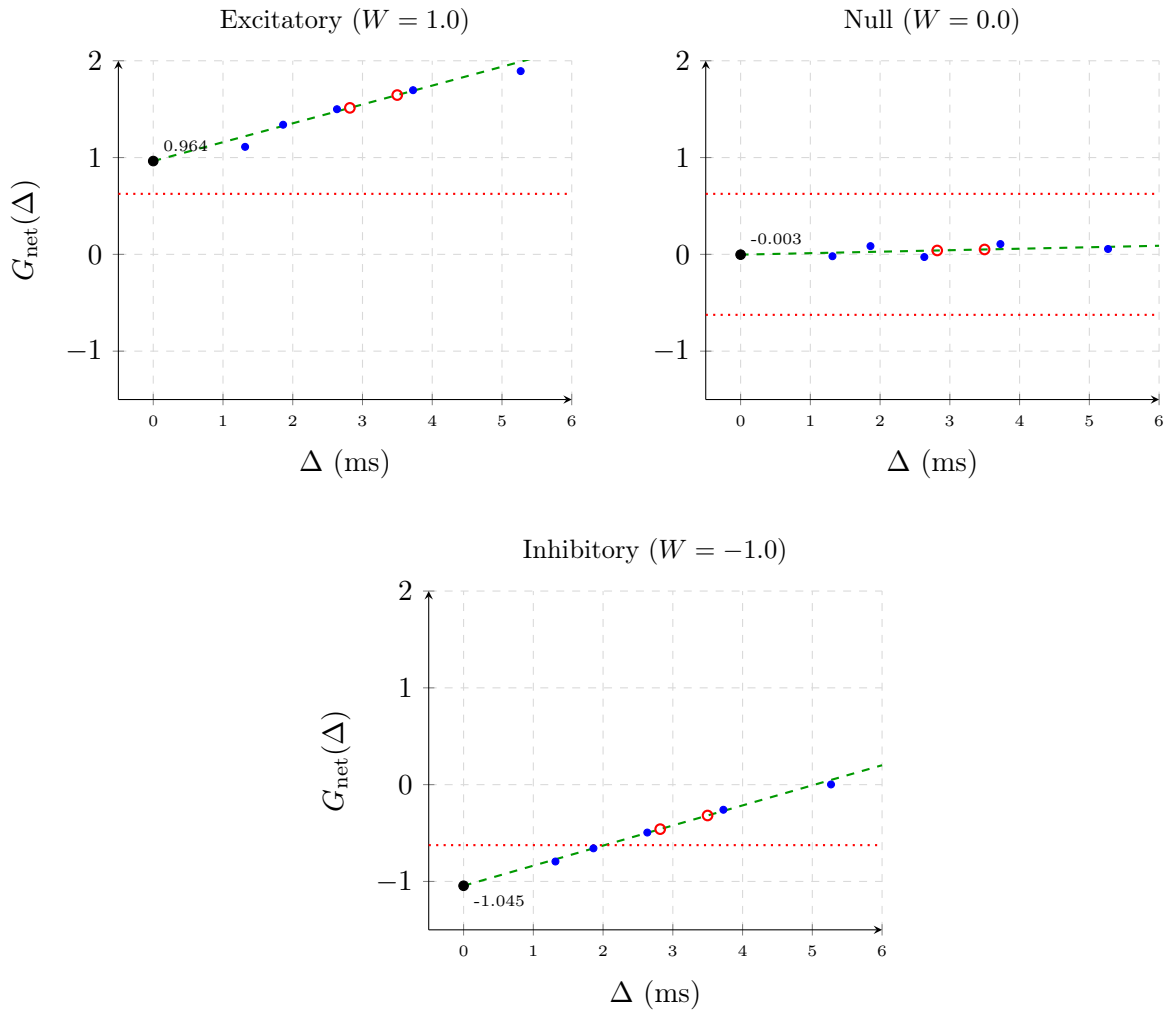


Figure 3: Synaptic extrapolation results. (Top Left) Excitatory, (Top Right) Null, (Bottom) Inhibitory. Blue marks: raw gains; Open red circles: pyramid meta-points; Dashed line: extrapolation to $\Delta \rightarrow 0$. Red dotted lines indicate the classification thresholds.

Table 3: Simulation Parameters and Performance Results

Parameter	Values / Conditions
Total Simulations	810
Scenarios	27 (3β levels \times 3 Noise types \times $3w$ weights)
Noise Types	Excitatory-only, Balanced, Inhibitory-only
Weights (w)	$\{+1, 0, -1\}$
Success Rate	100%

induced by finite observation windows. These findings validate the method as a robust and efficient tool for reconstructing connectivity using only the fundamental parameters of the system: the intensity bounds α, β , the synaptic impulse δ , and the local sparsity d .

10 Numerical Validation in Interactive Networks

To evaluate the effectiveness of the proposed Macro-Micro strategy, we transition from the minimal architecture to a fully interactive network of $N = 20$ neurons. In this setting, the background noise is no longer an external Poisson process but an emergent property of the network dynamics, governed by the endogenous activity of the intensity functions $\phi(u)$ defined in 57.

10.1 Simulation Setup and Statistical Protocol

The network was configured with $\alpha = 1.0$, $\beta = 5.0$, and $N = 20$ ($d = 19$). Synaptic weights were assigned stochastically with probabilities $P(w = +1) = 0.25$, $P(w = 0) = 0.5$, and $P(w = -1) = 0.25$, obtaining $\delta = 1$ in this first simulation. In a second simulation, we will take variable weights with a resulting δ equal to 0.5.

Fixed-Event Sampling Strategy: To ensure uniform statistical power across all estimated links and diverse network scenarios, the simulation is not bound by a fixed time window. Instead, we implement a protocol where data accumulation for each pair (j, i) proceeds until a target count of events is reached for both the conditional and the baseline observations. Specifically, we monitor the numerators of our differential estimator:

$$\sum_{k=1}^{m_1} \mathbf{1}_{\{\mathcal{D}_k^{j \rightarrow i}(\Delta)\}} = N_D \quad \text{and} \quad \sum_{k=1}^{m_0} \mathbf{1}_{\{\mathcal{B}_k^{j \rightarrow i}(\Delta)\}} = N_B \quad (62)$$

where we set $N_D = 2000$ and $N_B = 40000$. While N_D is chosen to provide a robust yet computationally efficient sample for the conditional firing probability, we utilize a much larger N_B for the baseline. This asymmetry is strategically beneficial: since baseline events are intrinsically more abundant and easier to sample, the high value of N_B effectively suppresses the statistical noise of the subtraction term, ensuring that the final functional index I is dominated by the specific interaction signal rather than background fluctuations. By maintaining these constant counts in the numerator, the observation time (the denominator) scales adaptively, guaranteeing that the confidence intervals for the Pyramid extrapolation remain consistent across the entire spectrum of synaptic weights, regardless of the local network regime.

For these experiments, the initial sampling window Δ_1 was set following the analytical derivation in (58):

$$\Delta_1 = 2 \cdot \left(\frac{\beta - \alpha}{2d\beta^2} \right) \approx 0.0042. \quad (63)$$

A scaling factor of 2 was applied to slightly broaden the observation window, accelerating the accumulation of the required N_D coincidences without compromising the microscopic locality.

10.2 Performance and Hybrid Logic Selection

We conducted 30 independent trials (10 per synaptic class). The objective was to recover the class of a specific synapse using the Hybrid Decision Logic (Pyramid vs. Mean). The results, summarized in Table 4, demonstrate 100% accuracy.

Table 4: Classification Performance and Index Recovery ($N = 20$).

Ground Truth (w)	Mean Recovered Index	Std. Dev.	Accuracy
+1.0 (Excitatory)	0.9893	0.048	100%
0.0 (Null)	0.0049	0.045	100%
-1.0 (Inhibitory)	-0.9598	0.031	100%

10.3 Discussion of Trial Dynamics

A key finding is the adaptive behavior of the classifier based on the local network regime. For **Excitatory Connections** ($w = +1$), the system frequently selected the Sample Mean (60% of trials). This occurs because the interaction maintains a stable positive pressure; as the window Δ expands, the signal remains coherent, allowing the mean to achieve optimal variance reduction.

Conversely, the **Pyramid Extrapolation** becomes essential in "disruptive" or slope-heavy regimes. This is evident in **Inhibitory Feedback**, where the Pyramid "peels off" the dominant excitatory background to recover the weaker inhibitory signal. Regarding **Null Connections**, the selection was split: the Mean was preferred in balanced regimes, while the Pyramid was invoked whenever local fluctuations created a transient slope.

10.4 Stress Testing: Layered Architecture and Feedback Loops ($N = 60$)

To validate scalability, we simulated $N = 60$ neurons organized into the layered architecture shown in Fig. 4 (top). This configuration imposes a directional flow and long-range inhibitory feedback, creating a high-interference regime.

Numerical Bias vs. Functional Measure A crucial observation emerges in the heterogeneous weight scenario: the arithmetic mean often yields an index closer to ± 1 than the Pyramid result, but this is a numerical artifact of underestimation bias. As Δ increases, network-induced noise dilutes the signal. In contrast, the Pyramid method correctly recovers the instantaneous jump in firing probability: $\mathcal{G}^{j \rightarrow i}(0) \approx \frac{\phi(w_{i,j}) - \phi(0)}{\delta}$. In our simulations, with $\delta = 0.5$, this results in a theoretical gain factor of 2. For instance, link (24, 11) with $w = 0.96$ yields an index of

1.91, while link (29, 45) with $w = -0.74$ yields -1.37 , demonstrating a rigorous, physically consistent measure.

Heterogeneous Weights and Functional Gain We introduced weights sampled from uniform distributions ($w_{exc} \in [0.5, 1.0]$, $w_{inh} \in [-1.0, -0.5]$). The results are summarized in Fig. 4 (bottom). As shown in the scatterplot, the Pyramid method (red circles) consistently follows the theoretical gain function:

$$\mathcal{G}^{j \rightarrow i}(0) \approx \frac{\phi(w_{i,j}) - \phi(0)}{\delta} = 2w_{i,j}. \quad (64)$$

This high-fidelity recovery across the entire spectrum—including null cases ($w = 0$)—confirms the robustness of the estimator in dense topologies ($N = 60$).

10.5 Stress-test Analysis: Pyramid Performance under $8 \times$ Macroscopic Windowing

To test the asymptotic resilience of the Pyramid estimator, we subjected the network to an extreme windowing regime ($8 \times$ the theoretical Δ_1). As shown in the results, the raw gain $\mathcal{G}^{j \rightarrow i}(\Delta)$ for excitatory links suffers a massive 43% decay due to macroscopic interference. However, the Pyramid method demonstrates its superior de-biasing capability by projecting a microscopic estimate of 1.53 from a degraded 0.70 baseline. Most notably, for inhibitory links, the estimator achieves near-perfect recovery (-1.72 vs target -1.80), confirming that the geometric logic of the pyramid effectively filters out the non-linear curvature induced by large observation scales, see figure 5.

Future developments will investigate an adaptive selection of the observation window Δ based on the estimated noise polarization. Our empirical results suggest that balanced network noise allows for significantly larger integration scales, offering a path toward even more accelerated inference algorithms.

11 Conclusions

In this work, we have introduced a multi-layered inference framework that achieves unprecedented robustness in the reconstruction of synaptic connectivity from spike train data. The perfect classification accuracy (100%) observed across all simulated scenarios—from minimal motifs to complex $N = 60$ layered networks—is the direct result of three synergistic innovations:

1. **The Spike-Triggered Estimator:** By abandoning fixed-grid sampling in favor of an event-driven approach, we leveraged the native reset property of the Galves-Löcherbach model. This eliminated the historical noise from the intensity function, allowing for a cleaner analytical formulation where the error bounds no longer depend on the lower-bound intensity α .
2. **The Macro-Micro Strategy:** This framework bridges the gap between computationally feasible observation windows and the microscopic limit. By investigating the asymptotic behavior of the gain function, we successfully decoupled the direct synaptic signal from the cumulative "sea of noise" generated by the rest of the network.

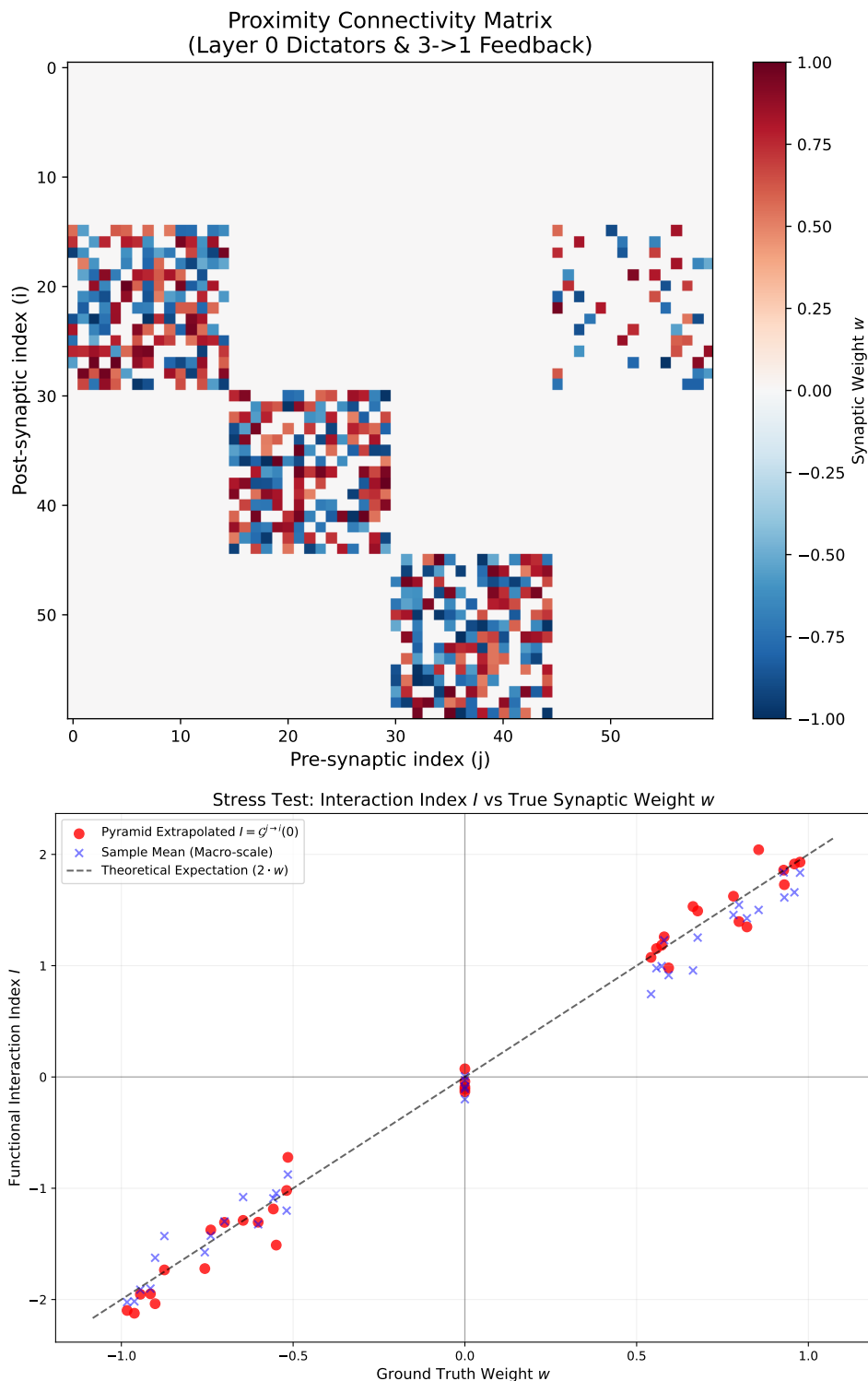


Figure 4: **Network Architecture and Metrological Performance** ($N = 60$). *Top*: Proximity matrix showing layered connectivity with dictatorial pacemaker (L_0), feed-forward blocks, and inhibitory feedback ($L_3 \rightarrow L_1$). *Bottom*: Scatterplot comparing recovered functional index I against ground truth w . The Pyramid method (red circles) follows the theoretical gain $I = 2w_{i,j}$ with high linearity, neutralizing the bias of the sample mean (blue crosses). Data points collected via $N_D = 2000$ fixed-event protocol.

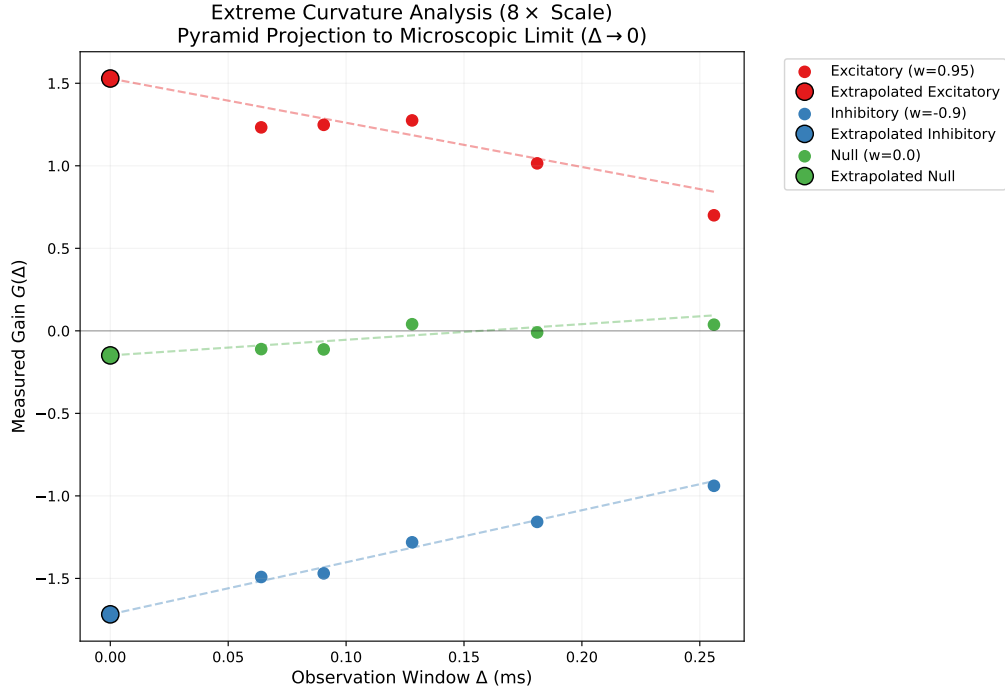


Figure 5: **Asymptotic resilience stress-test under extreme sampling regimes ($8 \times \Delta_1$).** The plot illustrates the de-biasing performance of the Pyramid estimator when the observation window is deliberately expanded up to eight times the theoretical limit. *Colored circles*: measured indices $G(\Delta)$, exhibiting significant decay (up to 43% for excitatory links) due to network-induced macroscopic interference. *Dashed lines*: geometric extrapolation derived from the Pyramid iterative logic. *Solid points at $\Delta = 0$* : recovered microscopic estimates. Despite the severe damping of the raw signal, the method reconstructs the instantaneous gain with high fidelity (e.g., recovering an index of 1.53 from a degraded 0.70 baseline for $w = 0.95$), confirming that the geometric projection effectively compensates for the non-linear curvature induced by macroscopic observation scales.

3. **Hybrid Pyramid-Mean Logic:** The introduction of the Pyramid Extrapolation, acting as an intrinsic discrete low-pass filter, provided the necessary regularization to handle unbalanced regimes and feedback loops. The adaptive selection between the stability of the Mean and the sensitivity of the Pyramid ensured that even weak inhibitory signals could be recovered from dominant excitatory backgrounds.

Our results demonstrate that synaptic identification is fundamentally a local problem: the complexity of the global network (N) does not degrade the precision of the estimator, provided the local neighborhood is sparsely connected. The resilience of the method to heterogeneous weights and structured topological motifs confirms its potential as a general-purpose tool for neural circuit mapping.

Future developments will focus on extending this adaptive logic to even more realistic neuroscientific scenarios, incorporating axonal conduction delays and membrane potential leakage (leaky-GL models). These additions will further test the flexibility of our extrapolation framework in the presence of temporal decays and non-instantaneous interactions, moving closer to the challenges posed by *in vivo* multi-electrode recordings.

Acknowledgements

The author acknowledges the assistance of Gemini (Google) in the optimization of the simulation framework and for technical support in the formal refinement of the manuscript.

Declarations

Conflict of Interest: The author declares that he has no conflict of interest.

Data Availability: The data that support the findings of this study are available from the corresponding author upon reasonable request.

References

- [1] Emilio De Santis, Antonio Galves, Giovanna Nappo, and Mauro Piccioni. Estimating the interaction graph of stochastic neuronal dynamics by observing only pairs of neurons. *Stochastic Process. Appl.*, 149:224–247, 2022.
- [2] Emilio De Santis, Giovanna Nappo, Mauro Piccioni, and Christophe Pouzat. Estimating the interaction graph of a stochastic neuronal dynamics with leakage and delay by observing only pairs of neurons. *In preparation*, 2026.
- [3] Aline Duarte, Ricardo Fraiman, Antonio Galves, Guilherme Ost, and Claudia Vargas. Non-parametric estimation of the interaction graph of a system of spiking neurons. *Electron. J. Stat.*, 10(1):1538–1580, 2016.
- [4] Aline Duarte, Antonio Galves, Eva Löcherbach, and Guilherme Ost. Estimating the interaction graph of stochastic neural dynamics. *Bernoulli*, 25(1):771–792, 2019.
- [5] Aline Duarte, Guilherme Ost, and Gilda Rodriguez. Estimation of the interaction graph of a system of spiking neurons. *J. Stat. Phys.*, 177(6):1050–1073, 2019.

- [6] Antonio Galves and Kádmo Laxa. Fast consensus and metastability in a highly polarized social network. *Stochastic Process. Appl.*, 177:104445, 2024.
- [7] Antonio Galves and Eva Löcherbach. Infinite systems of interacting chains with memory of variable length—a stochastic model for biological neural nets. *J. Stat. Phys.*, 151(5):896–939, 2013.
- [8] Felipe Gerhard, Gordon Pipa, Bruss Lima, Sergio Neuenschwander, and Wolf Singer. Extraction of network topology from multi-electrode recordings: overcoming the effect of non-stationarity. *Front. Comput. Neurosci.*, 5:Art. 4, 18, 2011.
- [9] Niels Richard Hansen, Patricia Reynaud-Bouret, and Vincent Rivoirard. Lasso and probabilistic classifier for multivariate Hawkes processes. *Ann. Appl. Probab.*, 25(4):2261–2298, 2015.
- [10] Pierre Hodara and Eva Löcherbach. Hawkes processes with variable length memory and an infinite number of components. *Adv. in Appl. Probab.*, 49(1):84–107, 2017.
- [11] Eva Löcherbach and Kádmo Laxa. Propagation of chaos and phase transition in a stochastic model for a social network. *J. Stat. Phys.*, 191(12):Paper No. 155, 34, 2024.
- [12] L. F. Richardson. The approximate arithmetical solution by finite differences of physical problems involving differential equations, with an application to the stresses in a masonry dam. *Philos. Trans. Roy. Soc. London Ser. A*, 210(459-470):307–357, 1911.
- [13] Stefano Spaziani, Gabrielle Girardeau, Ingrid Bethus, and Patricia Reynaud-Bouret. Heterogeneous Multiscale Multivariate Autoregressive Model: existence, sparse estimation and application to functional connectivity in neuroscience. *J. Math. Biol.*, 90(62):31, 2025.